

Faint, Large-scale H α Filaments in the Milky Way

L. M. Haffner

`haffner@astro.wisc.edu`

R. J. Reynolds

`reynolds@astro.wisc.edu`

S. L. Tufte

`tufte@astro.wisc.edu`

Department of Astronomy, University of Wisconsin–Madison

475 North Charter Street, Madison, WI 53706

ABSTRACT

During the initial data reduction of the Wisconsin H-Alpha Mapper (WHAM) H α Sky Survey, we have discovered several very long ($\sim 30^\circ$ – 80°) filaments superimposed on the diffuse H α background. These features have no clear correspondence to the other phases of the interstellar medium revealed by 21 cm, X-ray, IR, or radio continuum surveys, and they have no readily identifiable origin or source of ionization. In this letter, the data for two of these faint ($I_{H\alpha} \approx 0.5$ – 1.5 R) structures are presented. The first is an 80° -long, 2° -wide arch that extends nearly perpendicular to the Galactic plane at $\ell = 225^\circ$ and attains a maximum latitude of $+51^\circ$ near $\ell = 240^\circ$ before reaching the southern boundary of our survey map at $\ell = 270^\circ$, $b = +42^\circ$. The vertical portion of this feature between $b = +10^\circ$ and $+25^\circ$ is associated with a single radial velocity component centered at $v_{\text{LSR}} = +16$ km s $^{-1}$ with a full width at half maximum of 27 km s $^{-1}$. A decrease in the velocity is observed from $b = +33^\circ$ through $+48^\circ$ as the feature arches toward higher Galactic longitudes. At this end, the emission component is centered near $v_{\text{LSR}} = -20$ km s $^{-1}$. Where this feature appears to meet the Galactic plane near $\ell = 225^\circ$, it is directly above the H II region surrounding CMa R1/OB1. A second filament consists of a $\sim 25^\circ$ – 30° -long arc spanning $\ell = 210^\circ$ – 240° at $b = +30^\circ$ to 40° . The radial velocity of this feature increases systematically from 0 km s $^{-1}$ at $\ell = 215^\circ$, $b = +38^\circ$ to $+18$ km s $^{-1}$ at $\ell = 236^\circ$, $b = +28^\circ$. Both features have rather constant intensities along their entire lengths, ranging from 0.5–1.5 R (EM = 1–3 cm $^{-6}$ pc) with no obvious trends.

Subject headings: ISM: structure — Galaxy: structure — Galaxy: halo

1. Introduction

The Wisconsin H-Alpha Mapper¹ (WHAM) survey is providing the first velocity-resolved map of the H α emission from our Galaxy's diffuse interstellar medium. The combination of WHAM's sensitivity (< 0.1 R) and velocity resolution (12 km s $^{-1}$) reveals new details about the large-scale structure and kinematics of the Warm Ionized Medium (WIM). Studies of faint emission structures in the WIM may help us understand the distribution and morphology of the ionized gas and may even provide direct evidence of ionization sources. In this letter, we present the discovery of two large, faint filaments in our Galaxy.

¹<http://www.astro.wisc.edu/wham/>

2. Observations

WHAM consists of a dedicated 0.6-m, all-sky siderostat connected to a 15-cm, double-etalon Fabry-Perot spectrometer. The optical design delivers a spectrum covering a 200 km s^{-1} radial velocity interval from a one-degree circular patch of sky. For the $\text{H}\alpha$ sky survey, approximately 35,000 spectra were obtained above $\delta = -20^\circ$ with the one-degree diameter beam centered on a $0.98^\circ \times 0.85^\circ$ grid in ℓ and b . The integration time for each one-degree pixel was 30 seconds, resulting in a signal-to-noise ratio of about 30 in background continuum regions of the spectrum. This allows the detection of sources as faint as 0.1 R ($1 \text{ R} = 10^6/4\pi \text{ ph cm}^{-2} \text{ s}^{-1} \text{ ster}^{-1}$ or $2.4 \times 10^{-7} \text{ ergs cm}^{-2} \text{ s}^{-1} \text{ ster}^{-1}$ at $\text{H}\alpha$) in a single exposure. The etalons are configured to provide a spectral resolution of 12 km s^{-1} , which is sufficient to identify and remove atmospheric lines in the spectra and fully resolve the $\text{H}\alpha$ emission-line profiles from warm gas ($T \sim 8000 \text{ K}$) in the Galaxy. A detailed description of the instrument design is given by Tufte (1997).

Presented here are nearly 3800 of these spectra extracted from the WHAM $\text{H}\alpha$ Sky Survey. They cover the region of the sky from $\ell = 200^\circ$ to 270° and $b = -10^\circ$ to $+60^\circ$ above $\delta = -20^\circ$. Most of these spectra were observed by WHAM from 1997 February through 1997 May. These observations are designated “O1” below. A small portion (145 spectra) from $\ell = 253^\circ$ to 270° and $b = +47^\circ$ to $+60^\circ$ was observed in January 1998 and are labeled “O2” below. Standard WHAM data reduction, including bias subtraction, reflected ring subtraction, annular-summing, and flat fielding, was used to create these spectra (Haffner et al. 1998).

Atmospheric emission lines are a significant source of contamination in WHAM spectra. The brightest of these, with intensities ranging from 2–13 R, is the geocoronal $\text{H}\alpha$ line emitted in the earth’s upper atmosphere. Since the earth’s orbital velocity changes the location of the velocity frame of the Local Standard of Rest (LSR) with respect to the geocentric velocity frame, most directions in the sky were observed when the geocoronal line was separated by at least 20 km s^{-1} from the LSR. This separation makes it easy to resolve the relatively narrow (6–8 km s^{-1} FWHM) geocoronal line from the Galactic $\text{H}\alpha$ emission and minimize its effect. The data presented here have velocity separations of the geocoronal line from the LSR that range from -24 km s^{-1} to -42 km s^{-1} (O1) and $+14 \text{ km s}^{-1}$ to $+25 \text{ km s}^{-1}$ (O2). A single Gaussian component has been fitted and subtracted from these spectra to remove the geocoronal line.

Two other much fainter atmospheric emission lines, believed to be extremely weak OH emission, are present in the spectra. The first is located 71 km s^{-1} to the red of the geocoronal line ($v_{\text{LSR}} = +27$ to $+45 \text{ km s}^{-1}$ in O1); it has a width of 23.5 km s^{-1} and varies in intensity from 0.05 to 0.36 R. Deeper observations and the wide line width suggest that this feature may be a pair of atmospheric lines. The second is located 38 km s^{-1} to the blue of the geocoronal line ($v_{\text{LSR}} = -64$ to -82 km s^{-1} in O1); it has a width of 9.4 km s^{-1} and varies in intensity from 0.04 to 0.13 R. For this study, the red sky line provides the most contamination near the LSR in O1, and it has been removed by approximating it as a single Gaussian component. Variations in the line intensities are most severe from night to night. Our corrections account for intensity variations over 30-minute periods, which are typically 0.02 R. Other faint atmospheric lines are present in O2 even further to the blue from the geocoronal line. These features will not be discussed here since they do not affect our study near the LSR.

A first-order polynomial fits the sky background well within our 200 km s^{-1} bandpass. The typical level of the subtracted background is approximately $0.03\text{--}0.07 \text{ R} (\text{km s}^{-1})^{-1}$ or $1.4\text{--}3.2 \text{ R } \text{\AA}^{-1}$, which is dominated by atmospheric continuum emission above $|b| = 30^\circ$. Individual stars within the one-degree beam brighter than sixth magnitude contribute significantly to the background in several directions. Some of the spectra in these directions also contain an $\text{H}\alpha$ absorption line from the stars. These pointings are most noticeable in Figure 1 as isolated one-degree diameter depressions in the otherwise smooth emission

at higher Galactic latitudes.

Absolute intensity calibration is accomplished by frequent observations of nebular sources. All WHAM intensities are tied to the absolute intensity measurement of the North American Nebula (NAN; NGC 7000), 850 R within a 50' beam centered at $\ell = 85^{\circ}60$, $b = -0^{\circ}71$, as determined by Scherb (1981). Since we have yet to apply the gamut of intensity calibrations to our data, relative intensities quoted here are accurate to about 10%. The systematic uncertainty in the absolute scale (i.e., the intensity of NGC 7000) is believed to be approximately 15%.

3. Results

Figure 1 displays four velocity integrated images of H α emission from our selected region of the sky. The two filaments of interest are most easily seen in the narrow (12 km s $^{-1}$) velocity interval images, although their overall structure can also be seen on the “broad-band” map (Figure 1a). The vertical portion of the longest filament (hereafter Filament 1) is most prominent in the map centered on $v_{\text{LSR}} = +20$ km s $^{-1}$ (Figure 1d), stretching nearly perpendicular to the Galactic plane along $\ell = 225^{\circ}$. It then extends toward higher Galactic longitudes, turning over near $b = +50^{\circ}$ while shifting to more negative velocities in Figures 1c and 1b. A second long filament (Filament 2) can be seen as an arc extending across the images near $b = +30^{\circ}$ to $+40^{\circ}$. Its peak emission moves from $\ell = 220^{\circ}$ in the $v_{\text{LSR}} = -20$ km s $^{-1}$ map (Figure 1b) to $\ell = 235^{\circ}$ in the $v_{\text{LSR}} = +20$ km s $^{-1}$ map (Figure 1d). Other filaments are also apparent, including the feature running from $\ell = 205^{\circ}$, $b = +25^{\circ}$ to $\ell = 220^{\circ}$, $b = +30^{\circ}$. In this letter we focus primarily on the 80 $^{\circ}$ -long Filament 1.

An ℓ - v map is presented in Figure 2 along $b = +25^{\circ}$. From this representation, Filament 1 appears to be a narrow ($\lesssim 2^{\circ}$) feature at $\ell = 225^{\circ}$ that is offset in velocity from the smooth emission present near the LSR at other Galactic longitudes. An analysis of the spectra reveal that this velocity offset is about +18 km s $^{-1}$. The spectrum of Filament 1 averaged over six of the WHAM pointings taken around $\ell = 225^{\circ}5$, $b = +25^{\circ}5$ is displayed in Figure 3 as a dashed line. Because the velocity separation of the two components ($\Delta v \approx 20$ km s $^{-1}$) is less than the typical Doppler width of WIM H α lines (FWHM $\approx 20 - 30$ km s $^{-1}$), a straightforward two-component fit of this spectrum is not well constrained. Instead, we attempt to isolate the filament from gas near the LSR by subtracting an estimate of the general WIM contribution in this direction. The spectra of two “background” regions taken at the same Galactic latitude are also displayed in Figure 3 as dotted lines. These directions are averages of nine pointings around $\ell = 232^{\circ}0$, $b = +25^{\circ}5$ and 12 pointings around $\ell = 220^{\circ}5$, $b = +25^{\circ}5$. An average of these spectra is subtracted from the average filament spectrum to produce the final filament-only spectrum in Figure 3 (solid line). The resulting component is fit well by a single Gaussian with a mean of $+18 \pm 2$ km s $^{-1}$, a FWHM of 27 ± 6 km s $^{-1}$, and an intensity of 1.2 ± 0.2 R.

Using this method, we have determined fit parameters for several directions along Filament 1 and 2 and present the results in Table 1. Regions where the filaments cross are deliberately excluded. The accuracy of the filament component parameters depends primarily on how well the background regions represent the true emission near $v_{\text{LSR}} = 0$ km s $^{-1}$ in the filament direction. The errors of the parameters listed in Table 1 are conservatively estimated by examining subtractions of different background directions from the filament spectra. The fitting errors are an order of magnitude smaller and do not contribute significantly. Note the velocity gradients in both filaments with increasing Galactic longitude, decreasing from $v_{\text{LSR}} +18$ km s $^{-1}$ to -25 km s $^{-1}$ in Filament 1 and increasing from $v_{\text{LSR}} 0$ km s $^{-1}$ to $+18$ km s $^{-1}$ in Filament 2. Also note

the nearly constant H α intensities and line widths.

4. Discussion

The intensities in Table 1 are converted to emission measures using the formula:

$$\text{EM (cm}^{-6} \text{ pc)} = 2.75 T_4^{0.9} I_{\text{H}\alpha} \text{ (R)} e^{2.2 E(B-V)}, \quad (1)$$

where T_4 represents the temperature of the emitting gas in units of 10^4 K. With typical values for the temperature of the WIM gas, $T_4 = 0.8$ (Reynolds 1985), an H α intensity of 1 R corresponds to an EM of $2.25 \text{ cm}^{-6} \text{ pc}$. Since we are examining mostly high-latitude features, we expect corrections for interstellar extinction to be small. No such correction has been applied to the data presented here.

To derive further physical parameters for the filaments, we must make an assumption about the distances to them. Some evidence suggests that the lower part of Filament 1 is at a distance of about 1 kpc, based on its radial velocity and possible association with CMa R1/OB1. The lower portion has a radial velocity of $+16 \text{ km s}^{-1}$, which is consistent with a kinematic distance of approximately 1 kpc at this Galactic longitude for a value of Oort’s Constant $A = 16 \text{ km s}^{-1} \text{ kpc}^{-1}$ (Mihalas & Binney 1981). Unfortunately, this argument is weakened by the radial velocities of the filament’s high-latitude portion, which are “forbidden” in the Galactic rotation model. However, in Figure 1d ($v_{\text{LSR}} = +20 \text{ km s}^{-1}$), the vertical portion of Filament 1 appears to end in the prominent H II region surrounding the star-forming association CMa R1/OB1. In fact, the center of the brighter, arc-shaped, H α emission features in this H II region, as seen on the Palomar Sky Survey red plates, is at $\ell = 225^\circ$, $b = -1^\circ$ (Reynolds & Ogden 1978). Also, the velocity centroid of the H II region (Table 1) is similar to that of the first 15° – 20° of the filament away from the plane. Unless the agreement between the spatial and velocity information of these two regions is a coincidence, we can use the distance of the H II region as an estimate of the distance to the filament. The distance to the CMa OB1 association has been determined photometrically by Clariá (1974) to be $1150 \pm 140 \text{ pc}$, consistent with a kinematic distance of 800–1100 pc for the H α emitting gas in the region (Reynolds & Ogden 1978). In this letter, we adopt a distance of 1 kpc for Filament 1 but include $d_1 = d/1 \text{ kpc}$ in the derived parameters.

At a distance of 1 kpc, the vertical extent of Filament 1 ($b \approx +51^\circ$) translates to a vertical height above the Galactic mid-plane, Z , of $1200 d_1 \text{ pc}$ and a width ($\approx 2^\circ$) of $35 d_1 \text{ pc}$. If we assume the filament is a cylinder of uniform density gas of width L , then the emission measure,

$$\text{EM (cm}^{-6} \text{ pc)} = \int_0^L n_e^2 dl = n_e^2 L, \quad (2)$$

of the feature can be used to estimate the density. For Filament 1, where $L = 35 d_1 \text{ pc}$ and $\text{EM} \approx 1.1 \text{ cm}^{-6} \text{ pc}$, $n_e = 0.18 d_1^{-1/2} \text{ cm}^{-3}$. The typical column density through the filament is $N_e = 1.9 \times 10^{19} d_1^{1/2} \text{ cm}^{-2}$. The mass of the material in the filament’s vertical section can be estimated by $1.4 m_H Z L^2 n_e = 9.2 \times 10^3 d_1^{5/2} M_\odot$, where the factor 1.4 is a correction for helium. If the filament is photoionized, our observed EM implies an incident ionizing flux of at least $\alpha_B \text{ EM} = 1.0 \times 10^6 \text{ ph cm}^{-2} \text{ s}^{-1}$. The hydrogen recombination rate within the filament is given by $\alpha_B n_e^2 = 1.0 \times 10^{-14} d_1^{-1} \text{ cm}^{-3} \text{ s}^{-1}$, implying that the power required to sustain this rate throughout the volume of the filament is $(\alpha_B n_e^2 Z L^2) \times 13.6 \text{ eV} = 9.4 \times 10^{36} d_1^2 \text{ erg s}^{-1}$. The value of α_B used in these calculations, $3.10 \times 10^{-13} \text{ cm}^3 \text{ sec}^{-1}$, is interpolated from Osterbrock (1989) assuming a gas temperature of 8000 K.

The narrow shape and location of Filament 1, particularly the coincidence in location and radial velocity of one end of the filament with an energetic source in the plane (CMa R1/OB1), suggest one possibility for its origin—a jet-like ejection from the association. However, given the length of the filament at the distance of CMa R1/OB1, the apparently low velocities associated with it (Table 1), and the near constant H α intensity profile along its entire length, it is difficult to reconcile a scenario in which ionized hydrogen is being ejected from CMa R1/OB1 with the gas’s short recombination times. A parcel of ionized gas at these temperatures and densities will recombine in $t_r = (\alpha_B n_e)^{-1} = 1.8 \times 10^{13} d_1^{1/2} \text{ s} = 5.7 \times 10^5 d_1^{1/2} \text{ yr}$. To reach the observed height and remain ionized, the gas would need to be ejected at speeds in excess of $Z/t_r = 1400 d_1^{1/2} \text{ km s}^{-1}$. We see no evidence for such speeds in our data. Furthermore, we would expect a significant gradient in the filament’s intensity as a function of height above the Galactic plane, since gas at larger distances from the plane has had more time to recombine.

If another source is responsible for maintaining the ionization of Filament 1, an ejection scenario could still be plausible. If the filament’s arc shape is caused by free-fall of ejected gas back to the Galactic plane, an initial velocity of about 70 km s^{-1} is required to reach the observed height above the plane at the distance of CMa R1/OB1. Such speeds agree better with the measured filament component velocities in Table 1, particularly when projection effects are considered. However, the filament’s length would then require that the ejecting source be more than $3 \times 10^7 \text{ yr}$ old. This number can be compared to estimates of $3 \times 10^6 \text{ yr}$ for the age of CMa OB1 by Clariá (1974) and $7.6 \times 10^5 \text{ yr}$ for the age of a supernova put forth by Herbst & Assoua (1977) as being responsible for generating the ring-shaped H α nebulosity in the vicinity of CMa OB1/R1 and for being the progenitor of star formation in the R1 association. In this scenario, a diffuse ionization source is probably required to maintain a constant intensity along the filament, since the growing distance from CMa R1/OB1 would produce an intensity gradient if it were the sole source. The efficiency of leaking Lyman continuum radiation from the disk is a longstanding problem for ionizing a thicker layer of the Galaxy. However, Bland-Hawthorn & Maloney (1998), Dove & Shull (1994), and Miller & Cox (1993) have argued that a substantial ionizing flux can diffuse into the Galaxy’s halo from the disk. The required ionizing flux of at least $1.0 \times 10^6 \text{ ph cm}^{-2} \text{ s}^{-1}$ is consistent with these models.

Several other phenomena may produce large, faint filaments. Large-scale, kinematic Galactic structures such as superbubbles, chimneys, or worms have been popular explanations for filamentary structures seen in H I as well as H α (*e.g.* Koo, Heiles, & Reach 1992; Reynolds & Ogden 1979). The velocity gradient of Filament 1 is outside the range expected from a simple model of Galactic rotation and therefore may be evidence for a dynamical influence on the filament. However, the observed velocity gradient is inconsistent with this feature being the edge of an expanding shell, since a shell’s projected edges should be at a constant radial velocity. Furthermore, for the two cases presented here, we find no obvious correlation between these H α filaments and emission at other wavelengths, including H I 21 cm, Rosat All-Sky Survey X-Ray, and IRAS bands, making it difficult to relate them to previously identified H I “worms” and superbubbles. Since the Leiden/Dwingeloo H I survey is sensitive to below $5 \times 10^{18} \text{ cm}^{-2}$ (Harmann & Burton 1997), the ionized column density of the filament, $2 \times 10^{19} \text{ cm}^{-2}$, suggests that the gas is fully ionized. Other possibilities include a suggestion by Dupree & Raymond (1983) that faint, ionized trails of ionized hydrogen could be produced by high-velocity white dwarfs. However, the recombination time discussed above suggests unreasonable velocities for the star.

In summary, we present the discovery of two long, faint H α filaments at high latitudes from the WHAM H α survey. Their origin is not yet identified, but the existence of such features may help to explain processes responsible for the maintenance of the general WIM layer. As additional portions of the H α survey are reduced, new clues about the nature of these structures may be revealed. We plan to follow

these observations with [S II] and [N II] observations of this region. Additional observations will provide information about the gas's temperature and ionization state, which are useful in narrowing the kinds of processes that can be producing these filaments.

We thank Kurt Jaehnig and Jeff Percival of the University of Wisconsin's *Space Astronomy Lab* for their dedicated engineering support of WHAM; Nikki Hausen, Mark Quigley, and Brian Babler for data reduction support; and Trudy Tilleman for essential night-sky condition reports from Kitt Peak, which have made remote observing possible. We acknowledge the use of NASA's *SkyView* facility (<http://skyview.gsfc.nasa.gov>), located at NASA Goddard Space Flight Center and the SIMBAD database, operated at CDS, Strasbourg, France. This work is supported by the National Science Foundation through grants AST9619424 and AST9122701.

REFERENCES

- Bland-Hawthorn, J. & Maloney, P. R. 1998, *ApJ*, submitted
- Clariá, J. J. 1974, *A&A*, 37, 229.
- Dove, J. B. & Shull, J. M. 1994, *ApJ*, 430, 222.
- Dupree, A. K. & Raymond, J. C. 1983, *ApJ*, 275, L71.
- Haffner, L. M., Reynolds, R. J., & Tufte, S. L. 1998, in preparation
- Hartmann, D. & Burton, W. B. 1997, *Atlas of Galactic Neutral Hydrogen* (New York: Cambridge University Press).
- Herbst, W. & Assousa, G. E. 1977, *ApJ*, 217, 473.
- Koo, B.-C., Heiles, C., & Reach, W. T. 1992, *ApJ*, 390, 108.
- Mihalas, D. & Binney, J. 1981, *Galactic Astronomy: Structure and Kinematics*, 2nd edition (New York: W. H. Freeman & Co.).
- Miller, W. W., III & Cox, D. P. 1993, *ApJ*, 417, 579.
- Osterbrock, D. E. 1989, *Astrophysics of Gaseous Nebulae and Active Galactic Nuclei* (Mill Valley: University Science Books).
- Reynolds, R. J. 1985, *ApJ*, 294, 256.
- Reynolds, R. J. & Ogden, P. M. 1978, *ApJ*, 224, 94.
- Reynolds, R. J. & Ogden, P. M. 1979, *ApJ*, 229, 942.
- Scherb, F. 1981, *ApJ*, 243, 644.
- Tufte, S. L. 1997, Ph.D. Thesis, University of Wisconsin–Madison

Fig. 1.— A portion of the WHAM H α Sky Survey. These pseudo-color images show the integrated H α emission in four selected velocity bands. The axes are Galactic longitude and latitude. (a) $v_{\text{LSR}} = -60$ to $+60$ km s $^{-1}$. (b) $v_{\text{LSR}} = -26$ to -14 km s $^{-1}$. (c) $v_{\text{LSR}} = -6$ to $+6$ km s $^{-1}$. (d) $v_{\text{LSR}} = +14$ to $+26$ km s $^{-1}$. “Holes” in the images are pointings uncorrected for a bright stellar absorption line. (*Preprint Note:* A color PostScript version of this figure can be found at <http://www.astro.wisc.edu/wham/papers.html>)

Fig. 2.— Longitude-Velocity intensity map at $b = +25^\circ$. Contour levels are in units of 10^{-3} R (km s $^{-1}$) $^{-1}$. Filament 1 crosses $b = +25^\circ$ at $\ell = 225^\circ$.

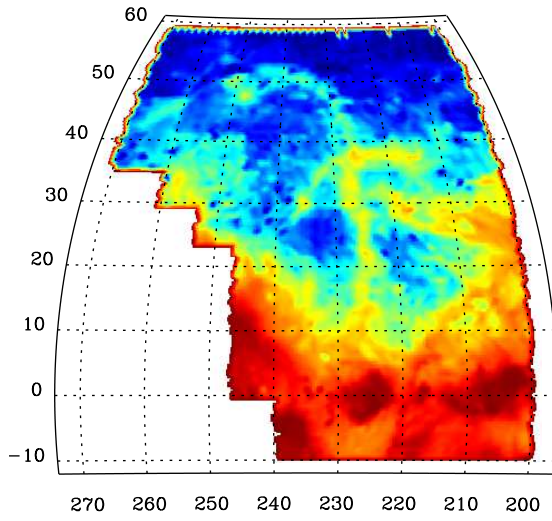
Fig. 3.— Filament and background spectra at $b = +25^\circ 5$. Intensity is plotted against v_{LSR} . Atmospheric lines have been removed. The dashed line is the original emission toward the filament, the dotted lines are two background directions, and the solid line is the background-subtracted filament emission (see text). The increased noise near -40 km s $^{-1}$ is a residual of the geocoronal H α line, whose peak emission is centered near that velocity.

Table 1. Fitted Filament Parameters

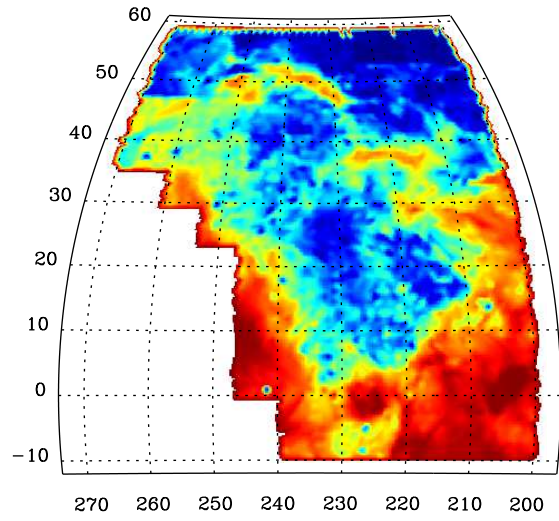
Position (ℓ, b)	# of Avg'd Spectra	Mean (km s ⁻¹)	FWHM (km s ⁻¹)	Intensity (R)
<u>Filament 1</u>				
(225°5, + 0°0) ^a	5	+14.0±0.1	32.5±0.1	59.1±0.1
(227°0, +10°2)	9	+18±2	23±4	0.9±0.1
(225°5, +12°7)	9	+16±2	24±4	1.1±0.4
(225°0, +15°3)	6	+18±2	22±3	0.6±0.1
(225°0, +17°8)	6	+16±3	26±6	0.6±0.2
(225°0, +20°4)	6	+16±1	33±2	1.4±0.1
(225°5, +25°5)	6	+18±2	27±6	1.2±0.2
(227°3, +33°1)	12	+9±3	20±2	0.6±0.1
(227°3, +35°7)	10	+6±1	22±1	0.5±0.1
(227°3, +38°2)	10	+4±3	25±2	0.5±0.4
(227°3, +40°8)	11	0±4	24±6	0.4±0.2
(227°3, +43°3)	11	-1±3	23±2	0.6±0.1
(229°3, +45°9)	9	-8±1	25±1	0.4±0.1
(231°6, +48°4)	11	-18±1	22±3	0.5±0.1
(234°0, +50°5)	7	-22±1	22±4	0.6±0.1
(239°0, +51°0)	9	-25±3	26±4	0.6±0.1
<u>Filament 2</u>				
(215°3, +36°5)	6	0±3	31±1	1.2±0.4
(217°8, +37°5)	6	-1±1	26±1	1.3±0.3
(220°5, +37°5)	6	-2±1	27±2	1.0±0.4
(230°3, +35°5)	6	0±4	22±6	0.4±0.2
(232°3, +34°8)	6	+1±1	29±1	0.7±0.1
(234°3, +33°0)	6	+13±1	31±1	0.4±0.1
(236°0, +30°5)	8	+18±2	37±1	1.0±0.1

^aThis direction is toward the H II region surrounding CMA R1/OB1.

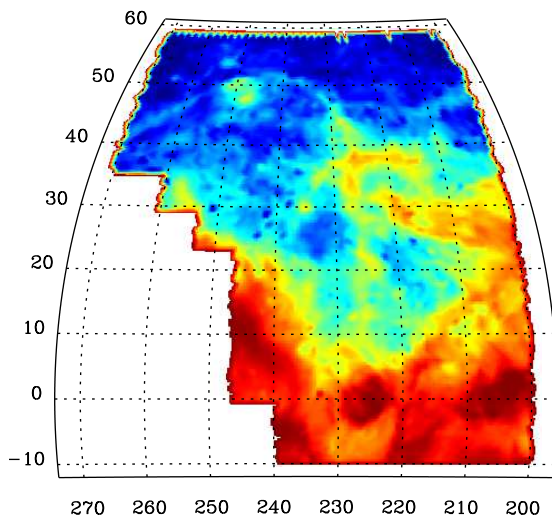
(a) -60 to $+60$ km s^{-1}



(b) -26 to -14 km s^{-1}



(c) -6 to $+6$ km s^{-1}



(d) $+14$ to $+26$ km s^{-1}

